THE JOURNAL OF PHYSICAL CHEMISTRY B

Article

pubs.acs.org/JPCB

# Influence of Surface Property on the Crystallization of Hentetracontane under Nanoscopic Cylindrical Confinement

Bong Seock Kim,[†] Young Gyu Jeong,[‡] and Kyusoon Shin*,[†]

[†]School of Chemical and Biological Engineering, Seoul National University, Seoul 151-742, Republic of Korea

[‡]Department of Advanced Organic Materials and Textile System Engineering, Chungnam National University, Daejeon 305-764, Republic of Korea

Supporting Information

**ABSTRACT:** The crystallization behavior and the orientation of linear alkane hentetracontane (C41) confined in cylindrical nanoporous alumina templates with different surface energies were investigated by non-isothermal crystallization and X-ray diffraction. The surface of pristine nanoporous alumina was modified to have low surface energy by grafting with polydimethylsiloxane. In the pristine nanoporous alumina, C41 crystallized at two crystallization temperature ranges, lower than bulk, and exhibited the decreased Avrami exponents. C41 in the surface-modified nanoporous alumina showed the inhibition of crystallization at higher temperature range among the two crystallization temperature ranges but the enhancement of crystallization at much lower temperature ranges than in the pristine nanoporous alumina. It was clearly shown that those variations of crystallization behavior imply the surface effect on crystallization. The crystal orientation was also affected by surface−modification of the alumina template. The *a*-axis of orthorhombic C41 crystals in the pristine nanoporous alumina was preferentially oriented parallel to the pore axis, while *b*- and *c*-axes were perpendicular to the pore axis. C41 crystals in the surface-modified nanoporous alumina showed two types of orientation. One was identical to that in the pristine nanoporous alumina, and the other was the orientation that the crystals were tilted with respect to the *c*-axis as the (110) plane parallel to the pore axis.

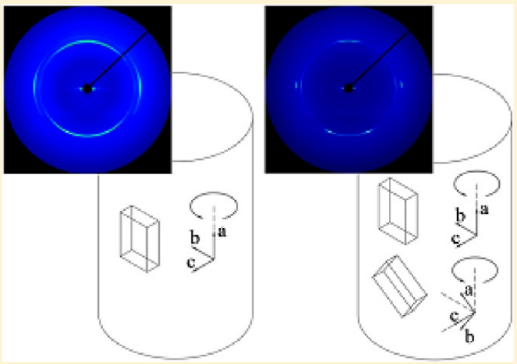


## INTRODUCTION

Materials in nanometer scale confinement exhibit different features from the bulk.[1−10] Relaxation,[1−3] phase transition,[4−6] structural perturbation,[7−9] and mobility[10] of materials confined in nanoscopic geometries have aroused increasing interest. Crystallization of semicrystalline organic materials has been investigated intensively, because the crystalline domains give a significant effect on their physical properties. Understanding the crystallization behavior of organic materials under nanoscopic confinement is crucial to the potential applications.

The crystallization of semicrystalline organic materials has been investigated under various nanoscopic constrained environments such as ultrathin films,[11,12] microdomains of diblock copolymers,[13−16] organic templates,[9,17,18] and inorganic templates.[4−6,17,18] These studies have revealed that the crystallinity of semicrystalline materials was reduced and the orientation of them was altered upon the imposition of nanoscopic confinement. It is clear that tuning the property and crystalline structure of materials in confined geometry is important and increasingly demanded in the usage of nanoscopic crystalline materials. Thus, study on the crystallization of materials under confinement, which would determine the crystalline structure and property, has started recently, and efforts on the understanding of the crystallization under confinement has been made.

Despotopoulou et al. reported that the crystallization rate of ultrathin poly(di-*n*-hexylsilane) films on a quartz surface modified using an octadecyltrichlorosilane was faster than on glass substrates due to the attractive interfacial interaction between the polymer and substrate.[12] Hillmyer and co-workers have reported the preferred orientation behaviors for organic compounds confined in the cylindrical nanopores of controlled porous glass or porous polymer monoliths.[9,17] They explained that critical size effects and surface energy considerations, which were induced by the interfacial interaction between material and substrate, affected the fast growth directions of organic compounds. Crystallization of polyethylene confined in nanoporous alumina was also investigated.[4,19] It was suggested that homogeneous nucleation dominated in larger pores, whereas heterogeneous nucleation induced by surface prevailed in relatively smaller pores. Diao et al. showed angle-directed nucleation, which implied the surface-induced crystallization, by investigating the crystallization of aspirin confined in different shapes of templates fabricated by nanoparticle imprint lithography.[8] Those studies show that crystallization in

**Received:** August 31, 2012
**Revised:** April 3, 2013





dx.doi.org/10.1021/jp308678b | *J. Phys. Chem. B* XXXX, XXX, XXX−XXX

Scheme 1. Schematic Route to Anodized Nanoporous Alumina Containing C41 in the Pores

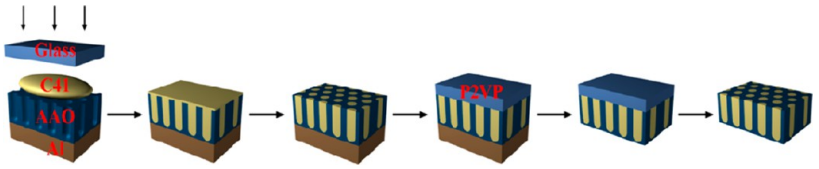


nanoscopic spaces happens majorly by surface-induced nucleation.

On the other hand, as a dominant crystallization mechanism under confinement impurity-induced heterogeneous nucleation or homogeneous nucleation with the decrease of confining volume was also suggested. Loo et al. have reported that homogeneous nucleation was dominant for the crystallization of polyethylene confined in the spherical microdomains of diblock copolymers.[14] Massa et al. have reported the crystallization of poly(ethylene oxide) confined to droplets,[20,21] and their works showed that the probability of nucleation depended on the volume of droplets rather than surface area. Duran et al. have investigated the crystallization of isotactic polypropylene confined to nanoporous alumina and suggested the variation of nucleation mechanism from heterogeneous to homogeneous nucleation as considering the impurity densities in individual nanopores.[5]

It is probable that a large portion of interface, enclosing the small amount of the crystallizable material, would influence the whole crystallization of nucleation as well as crystal growth. As mentioned above, some of previous studies show that crystallization under nanoscopic confinement is surface-induced, while some others describe homogeneous nucleation. Yet more studies on the effect of interface on the crystallization are needed to be performed in order to understand the influence of interface further. One way of doing this is available by the usage of a material that crystallizes mainly by homogeneous nucleation in bulk, since surface effect can be clearly examined by confining that material, and comparing the crystallization behavior in a small space with that in bulk. In this aspect, it may appear unfortunate that most materials in bulk crystallize mainly via crystal growth. However, it can be circumvented by confining materials in nanoscopic spaces. It is because confinement would suppress crystal growth and make nucleation dominant. Some of short linear alkane molecules like hentetracontane (C41) can be a good candidate. While most materials including polymers are known to crystallize via heterogeneous nucleation, C41 is known to exhibit homogeneous nucleation and growth-dominance for extended chain crystal.[22−28] In this study, the crystallization and the structure of C41 confined in nanoporous alumina is explored. To examine the effect of surface, we modified the surface of the pristine nanoporous alumina to have low surface energy by coating with polydimethylsiloxane (PDMS) and investigated the crystallization behavior of C41. Linear alkanes were used to be studied as model materials for polymers sometimes,[23,26,29] because they have same backbone with PE and are thus treated as the oligomers of PE. So, it is also interesting to compare the crystallization behavior of the linear short alkane with that of PE under the nanoscopic confinement. Nanoporous alumina has been used as templates that have excellent thermal and mechanical properties. Also, the unique porous structure that is aligned unidirectionally perpendicular to the surface of the AAO template provides precise analysis of crystal orientation with respect to the pore axis.

## EXPERIMENTAL SECTION

**Materials and Sample Preparation.** We purchased hentetracontane (C41, ≥99.0%) from Fluka. C41 was used without further purification. Hexagonally packed nanoporous alumina (AAO) templates were synthesized via the well-known two-step anodization of high-purity aluminum sheets (99.999%, Goodfellow) and pore-widening.[30−34] The morphologies and the pore diameters of AAO templates were measured using field-emission scanning electron microscope (FE-SEM, JEOL JSM-6701F). In order to investigate the effect of surface energies of AAO templates on the crystallization of C41, some of pristine templates were coated with PDMS ($M_n$ = 5000 g/mol, Aldrich).[35,36] For the purpose of surface modification, the pristine AAO template was treated by $O_2$ plasma using reactive ion etcher (RIE, South Bay Technology, Inc. RIE-3000) to generate the hydroxyl group on the pore surface. Then, the template was immersed in 0.5 wt % 3-amino-propyl triethoxysilane (APTES, 99%, Aldrich) in methanol for 10 min. After rinsing and drying, the template was treated with monoglycidyl ether terminated PDMS at 80 °C for 4 h, and then it was rinsed with isopropanol to remove the residual PDMS. Contact angle of C41 on alumina was measured at about 100 °C. The C41 liquid was dropped on the back side of the pristine and surface-modified AAO templates to avoid the influence of alumina nanopore existence on contact angle. After surface modification, the contact angles of C41 on the backside of pristine and surface-modified AAOs were observed to be 10.4 and 49.2°, respectively (Supporting Information Figure S1). The diameter change due to the surface-modification by PDMS was found to be negligible, since the diameter of AAO is much larger than the thickness of the grafted PDMS (Supporting Information Figure S2). Quantitative information on the surface coverage of PDMS on pore wall could not be obtained.

Scheme 1 shows a schematic illustration of the sample preparation. The infiltration of C41 into the nanopores of the pristine and surface-modified AAO templates was done by placing C41 on the surface of the templates in a vacuum oven at 120 °C for 2 h. C41 was slightly pressed with flat glass for good contact between C41 and AAO. Removal of excess C41 on the surface of AAO templates was done by wiping carefully with cotton paper, which was confirmed with atomic force microscopy (AFM, SII NanoTechnology, Inc. SPA-300HV). Before eliminating the aluminum, we covered the entrance of the nanopores with poly(2-vinylpyridine) (P2VP, $M_w$ ∼100 000 g/mol, Scientific Polymer Products, Inc.) by slightly pressing P2VP film at 150 °C for 30 min under vacuum to avoid the chemical damage of C41 during the Al removal. P2VP film was prepared by solution-casting on a glass slide (thickness >100 μm). The supportive aluminum was eliminated by immersing the templates into the cupric chloride solution. Then, the P2VP was removed by immersing the assembly in ethanol at room temperature for a week. Infiltration of C41 was confirmed using FE-SEM (Supporting Information Figure S3).


dx.doi.org/10.1021/jp308678b | J. Phys. Chem. B XXXX, XXX, XXX−XXX

**Nonisothermal Crystallization.** The crystallization behaviors of C41 in bulk or in AAO templates were investigated with the aid of differential scanning calorimeter (DSC, Perkin-Elmer DSC7). DSC was calibrated with indium and zinc before use. The mass of C41 in the nanoporous alumina was calculated based on the total area of the AAO templates in the pan and the pore volume fraction of each template. In performing nonisothermal crystallization experiments, the samples were heated to 120 °C and held for 5 min to erase thermal history, and then they were cooled to 30 °C with different cooling rates, ranging from 1 to 10 °C/min.

**X-ray Diffraction.** The crystal structure and crystallization behaviors of C41 in the nanoporous alumina were characterized using a synchrotron radiation facility, 4C beamline of Pohang Light Source (PLS-II, Pohang, Republic of Korea, bending magnet type, critical energy: 10 KeV at 3.0 GeV). The wavelength, $\lambda$, of X-ray beam was 0.675 Å monochromatized by a Si (111) double-crystal monochromator. The beam size at the sample position was horizontal of 500 $\mu$m and vertical of 100 $\mu$m. The X-ray diffraction (XRD) patterns were measured with two-dimensional (2D) charge-coupled device (CCD) camera (2048 × 2048 pixels). The sample-to-detector distance was approximately 20 cm. The diffraction patterns were calibrated with silver behenate. To investigate the crystal structure and orientation, the alumina templates filled with C41 were rotated to the angle $\psi$ of 0, 20, 40, and 60° using goniometer. The samples were cooled from 120 to 30 °C at a rate of 0.5 °C/min in a vacuum oven before XRD measurements to apply identical thermal history to all samples. The schematic geometry of XRD measurements is shown in Scheme 2.

**Scheme 2. X-ray Diffraction Geometry to Measure the Orientation of C41 Crystals in the AAO[a]**

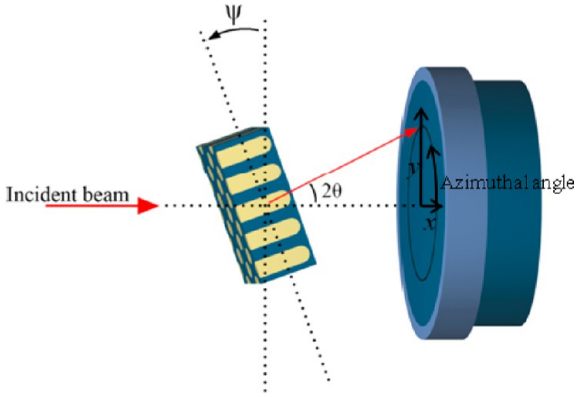


[a]The angle $\psi$ was varied from 0 to 60° to investigate the orientation of C41 crystals in the pristine and surface-modified AAO.

## RESULTS AND DISCUSSION

**Nonisothermal Crystallization Kinetics.** DSC cooling thermograms for C41 in bulk and in the pristine and surface-modified alumina nanopores at a cooling rate of 10 °C/min are shown in Figure 1. C41 in bulk has a sharp crystallization at 75−80 °C. In contrast, C41 in nanopores of the pristine and surface-modified AAOs shows crystallization exothermic peaks at two temperature ranges of 50−60 and 65−80 °C. The heat of crystallization ($\Delta H_c$) for each exothermic peak is shown in Table 1. The whole crystallinity of C41 in the pristine and surface-modified AAOs was much lower than that of C41 in the bulk. Nonetheless, the whole crystallinity of C41 in the surface-modified AAOs was lower than that in the pristine AAOs. These results indicate that the whole crystallization of C41 is strongly affected by the surface property as well as the confinement. On the other hand, it was found that for the surface-modified AAOs the crystallization transition at lower temperature of 50−60 °C is much stronger than that at higher temperature of 65−80 °C. Especially, in the surface-modified AAO with 20 nm diameter the crystallization at higher temperature is not detected and only the crystallization at lower temperature is observed. In the case of polymers confined in nanoporous AAOs, the change of the crystallization mechanism was reported. It was found that the crystallization of polyethylene under nanoscopic cylindrical confinement changes from homogeneous to heterogeneous nucleation by surface-induced nucleation with decreasing the pore diameter.[4] In the mean time, Duran et al. explained the crystallization of polypropylene under nanoscopic cylindrical confinement as change from heterogeneous to homogeneous nucleation with decreasing the pore diameter on the basis of impurity density.[5] It was reported that the surface energy affected the crystallization of syndiotactic polystyrene.[6] It was suggested that the nanoscopic confinement affected the surface-induced crystallization but the low energy surfaces suppressed the surface nucleation. If C41 left outside of the pore, crystallization peaks of C41 would have appeared at a temperature similar to bulk. So, it is more probable that existences of two separated crystallization peaks imply different crystallization mechanism for each peak. Comparing the areas of exothermic peaks of both templates, it is obvious that the crystallization of C41 in the pristine AAO is governed by the crystallization mechanism at higher crystallization temperature peak and the crystallization of C41 in the surface-modified AAO is dominated by the crystallization mechanism at lower crystallization temperature peak. It is clear that the surface-modification influences crystallization mechanism significantly, considering that the dominant crystallization temperature changes by the variation of surface property. Since C41 in nanopores is enclosed by alumina in such a small space, there are large areas of alumina that are intact with C41. Therefore, the surface can be of significance in the crystallization of C41.

DSC heating thermograms for C41 in bulk and in nanopores of the pristine and surface-modified AAOs at a cooling rate of 10 °C/min are shown in Figure 2. Both pore diameter and surface modification affect the melting of C41 on heating. As compared to bulk, melting transition becomes broader. C41 is known to form fully extended crystallites in bulk.[22,23,25,26] On the basis of our XRD experiments, we found that C41 forms also fully extended crystallites in the straight nanopores of AAO. The melting temperature is determined by crystal size, following Gibbs-Thompson equation. In 20 nm pore, the size of the C41 crystal seems smaller than other diameter pores, and the melting appears at lower temperatures. The size of fully extended-chain crystal is expected to be varied by the confinement. It is thought that melting transition of C41 confined in AAOs, broader than bulk, was caused by the size distribution of extended chain crystallites,. The size of the crystallite is thought to be broadened owing to perturbation by the cylindrical confinement. The crystallization behaviors of C41 were further analyzed by nonisothermal crystallization.

The Ozawa equation[37] for nonisothermal crystallization is given as


dx.doi.org/10.1021/jp308678b | J. Phys. Chem. B XXXX, XXX, XXX−XXX

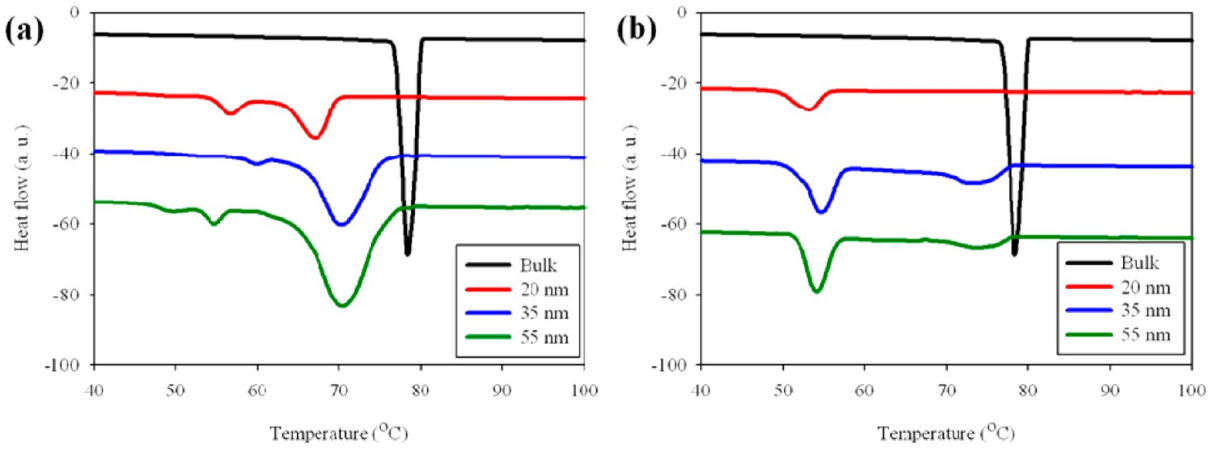


**Figure 1.** DSC cooling thermograms of C41, crystallized at a cooling rate of 10 °C/min, in bulk and in nanopores. (a) Pristine AAO and (b) PDMS surface-modified AAO.

**Table 1. Avrami Constants, Exothermic Heats, and Crystallinity Obtained from the Nonisothermal Crystallization of C41 in Pristine AAOs, Surface-Modified AAOs, and Bulk**

| | temperature range, °C | Avrami exponent $n$ | crystallization rate constant[a] $K$ | $\Delta H_c$[b], J/g | crystallinity, % |
|---|---|---|---|---|---|
| bulk | 75−85 | 2.3−2.8 | 3.65 | 253.0 | 96.5 |
| pristine AAO, $d$∼20 nm | 65−80 | 1.0−2.0 | 2.33 | 95.8 | 46.0 |
| | 50−60 | 1.5−3.6 | 2.79 | 24.7 | |
| pristine AAO, $d$∼35 nm | 65−80 | 0.8−1.8 | 1.75 | 131.0 | 51.0 |
| | 50−60 | 1.5−4.3 | 2.84 | 2.88 | |
| pristine AAO, $d$∼55 nm | 65−80 | 1.1−1.7 | 1.42 | 147.0 | 58.2 |
| | 50−60 | 2.2−4.8 | 2.10 | 5.77 | |
| surface-modified AAO, $d$∼20 nm | 50−60 | 0.8−1.4 | 1.97 | 64.8 | 24.7 |
| surface-modified AAO, $d$∼35 nm | 65−80 | 0.9−1.9 | 2.08 | 24.8 | 30.2 |
| | 50−60 | 1.7−3.0 | 2.01 | 54.4 | |
| surface-modified AAO, $d$∼55 nm | 65−80 | 1.2−1.8 | 1.52 | 11.9 | 20.6 |
| | 50−60 | 2.7−3.6 | 1.79 | 42.1 | |

[a]Crystallization rate constant was calculated using the average value of Avrami exponents. [b]Heat of crystallization was calculated from Figure 1.

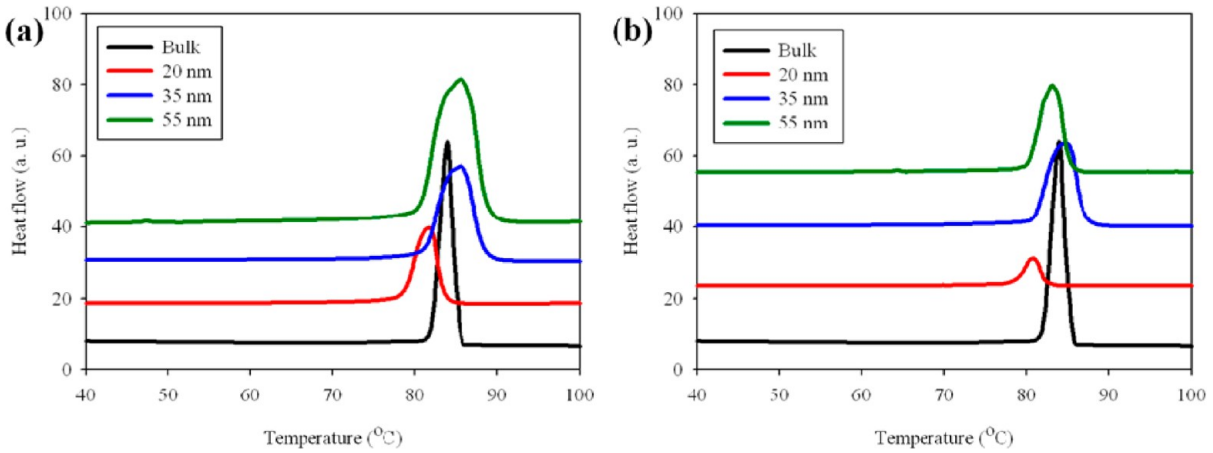


**Figure 2.** DSC heating thermograms of C41 crystallized in the bulk and in the pristine AAO (a) and surface-modified AAO (b) at a heating rate of 10 °C/min.

$$1 - X_{c,r} = \exp\left(\frac{-\kappa(T)}{|\lambda|^n}\right) \quad (1)$$

where $X_{c,r}$ is the relative crystallinity, $\kappa(T)$ is the cooling crystallization function as a function of temperature $T$, and $\lambda$ is constant cooling rate. $n$ is the Ozawa index (or the Avrami exponent), which depends on the growth dimensions and the nucleation mechanisms. Taking the logarithm of eq 1 twice leads to

$$\ln[-\ln(1 - X_{c,r})] = \ln(\kappa(T)) + n \ln\left(\frac{1}{|\lambda|}\right) \quad (2)$$

The $n$ value and $\kappa(T)$ can be determined from the slope and the intercept of the plot of $\ln[-\ln(1 - X_{c,r})]$ versus $\ln(1/|\lambda|)$,


dx.doi.org/10.1021/jp308678b | J. Phys. Chem. B XXXX, XXX, XXX−XXX

respectively. On the calculation of the $n$, the $n$ was determined by applying the $X_{c,r}$ lower than 0.5 because the higher $X_{c,r}$ can be significantly affected by crystal growth and lead to the low $n$.[22] Otherwise, $\kappa(T)$ can be calculated from the half crystallization temperature $(T_{1/2})$ where phase conversion becomes 50%, as follows[22,38]

$$\kappa(T_{1/2}) = \ln(2)|\lambda|^n \tag{3}$$

The Ozawa equation can be related to the Avrami equation.[39,40] The Avrami equation for isothermal crystallization is expressed as[41]

$$1 - X_{c,r} = \exp[-K(T)t^n] \tag{4}$$

where $K(T)$ is the crystallization rate. From the relationship between the Ozawa equation and the Avrami equation, Wasiak[42] derived the relationship between $\kappa(T)$ and $K(T)$, as follows

$$K(T) = \frac{-\mathrm{d}[-\kappa(T)^{1/n}]}{-\mathrm{d}T} \tag{5}$$

Equation 5 allows the determination of $K(T)$ by differentiating the known value of $\kappa(T)$ from nonisothermal crystallization experiments.

As can be seen in Table 1, the $n$ for C41 in bulk was found to be comparable to that reported by Hammami and Mehrotra.[22] From the result, it is valid to contend that the crystallization mechanism of C41 in bulk is dominated by the homogeneous nucleation and crystal growth as literature. On the other hand, the $n$ of C41 in nanopores differs from the bulk value. However, these values for higher and lower crystallization temperatures in Figure 1 show similar trend for both templates except the surface-modified AAO of 20 nm. From the calculation using the crystallization at higher temperature range that is dominant for C41 in the pristine AAOs, the $n$ of 0.8−2.0 was smaller than the bulk value of 2.3−2.8. It is probable that the smaller $n$ comes from the restriction of growth dimension owing to the two-dimensional constraint of the straight AAO nanochannels, although there is a possibility that interaction between the substrate surface and C41 also play an important role. According to the crystallization of polymers in the confined geometries, the dominating nucleation was explained for the decrease of the $n$ values in the polymer thin films[11] or in the nanospheres of semicrystalline−amorphous diblock copolymer.[14] However, considering the $K$ values, a function of nuclei density, it is not understandable that the nuclei density of C41 confined in AAOs is comparable to that in bulk. This apparent discrepancy comes from combining theories that makes quantitative analysis difficult. But it is certain that the confinement of nanopores makes C41 crystallize differently from bulk and the variation of degree of confinement changes the crystallization of C41. Moreover, the surface-modification of AAO nanopores with PDMS influences the crystallization behavior and the overall crystallinity of C41.

The calculation shows that, using the crystallization at lower temperature where crystallization of C41 confined in the surface-modified AAOs is dominant, the variation of the $n$ was as large as 1.5−4.3. From the viewpoint of surface energy, it is reported that the low surface energy suppresses surface-induced nucleation significantly, while high surface energy causes surface-induced nucleation.[6,43] So, the low surface energy of the surface-modified AAOs seems to suppress the crystallization of C41 at higher temperature. To overcome the large energy barrier, large degree of undercooling is required for the effective crystallization of C41 in the surface-modified AAOs. The crystallization transition of C41 in the surface-modified AAO of 20 nm diameter is different from the transition of C41 in other templates at lower temperature. Combining with the XRD results, shown in the following section, crystallization seemed to be limited at higher temperature due to low surface energy, just as crystal growth was inhibited and directed by strong constraints of small nanopores. Therefore, the Avrami exponent was influenced by the surface energy and the orientation-directing confinement. The crystallization of C41 in the pristine AAO happened more dominantly at the higher temperature range of 65−80 °C, whereas C41 in the surface-modified AAOs crystallized mainly at the lower temperature range of 50−60 °C. In the previous research,[6,43] a surface with a low-surface free energy suppresses surface-induced nucleation. Considering that C41 has higher contact angles in the surface-modified AAOs (~49.2° at 100 °C) and higher temperature crystallization peak becomes smaller after surface modification, crystallization in the higher-temperature ranges (65−80 °C) is thought to be due to surface-induced nucleation. In the case of the surface-modified AAOs, the low surface energy of the surface is thought to restrict the crystallization of C41 at the higher temperature of 65−80 °C and render the crystallization with high undercooling at the lower temperature range of 50−60 °C.

There is another clue supporting that crystallization in the higher temperature ranges (65−80 °C) is due to surface-induced nucleation. The crystallization peaks at the higher temperature ranges (65−80 °C) are getting smaller with the decrease of pore diameter and even disappeared in the surface-modified AAOs. C41 nanorods, enclosed by either pristine or surface-modified AAOs, can be divided into two regions, bulklike core and interfacial region. Bulklike core would influence homogeneous nucleation, while nucleation near the interface would be influenced by surface. Interface or surface effect would become more and more dominant, as the diameter of the C41 nanorod and the bulklike core becomes smaller. Thus, on the consideration of the possibility that surface effect would suppress the surface-induced nucleation more strongly in the smaller surface-modified alumina pore, the crystallization at the higher temperature regime (65−80 °C) would be owing to surface-induced nucleation. However, an opposite conjecture might be made; as the diameter becomes smaller, the effect of interface can be dominant, but the crystallization peaks at the higher temperature ranges are disappearing. So, it may imply that the crystallization at the higher temperature range could happen mainly via homogeneous nucleation. But it is less realistic, considering that the crystallization peaks at higher-temperature ranges in the pristine AAO get smaller also with the decrease of pore diameter. The decrease of the crystallization at the higher temperature range in the surface-modified AAOs would be caused by the suppression of crystallization that appears commonly in the crystallization under nanoscopic confinement. It is too early to have a concrete conclusion at this time as to whether the crystallization, occurring at the higher temperature range (65−80 °C) is due to surface-induced nucleation or not since more clear experimental evidence are not provided. Nevertheless, the influence of surface on the crystallization mechanisms of C41 under nanoscopic confinement is found to be obvious through the examination of this system. It is also worthy to note that the crystallization behavior of small sized


dx.doi.org/10.1021/jp308678b | J. Phys. Chem. B XXXX, XXX, XXX−XXX

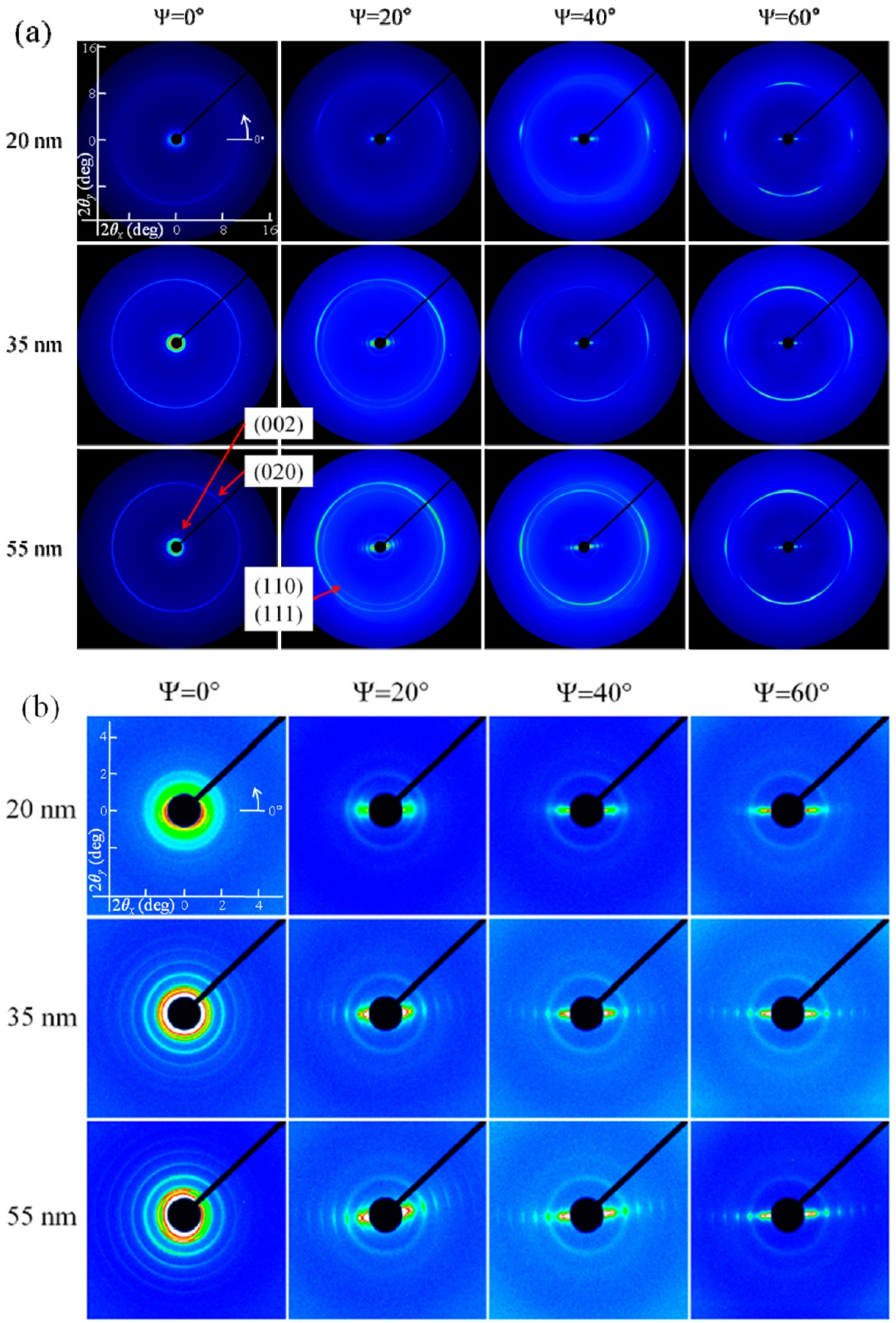


**Figure 3.** X-ray diffraction patterns of C41 crystallized in the pristine AAOs with different nanopore diameters; (a) full scale and (b) zoom of (a) to show low $2\theta$ region.

C41 molecules is quite different from linear polyethylene, although their backbone structure is similar.

**Crystal Orientation.** The XRD experiments were carried out to investigate the orientation of C41 in the nanopores of pristine and surface-modified AAOs. In the bulk, the C41 crystals form orthorhombic lattice with $a$ = 4.96 Å, $b$ = 7.42 Å, and $c$ = 108 Å. Figures 3 and 4 show the $\psi$-dependent XRD patterns for C41 in the pristine and surface-modified AAOs of different pore diameters, respectively. As shown in Scheme 2, the XRD patterns at $\psi = 0°$ were obtained by aligning the long


dx.doi.org/10.1021/jp308678b | J. Phys. Chem. B XXXX, XXX, XXX–XXX

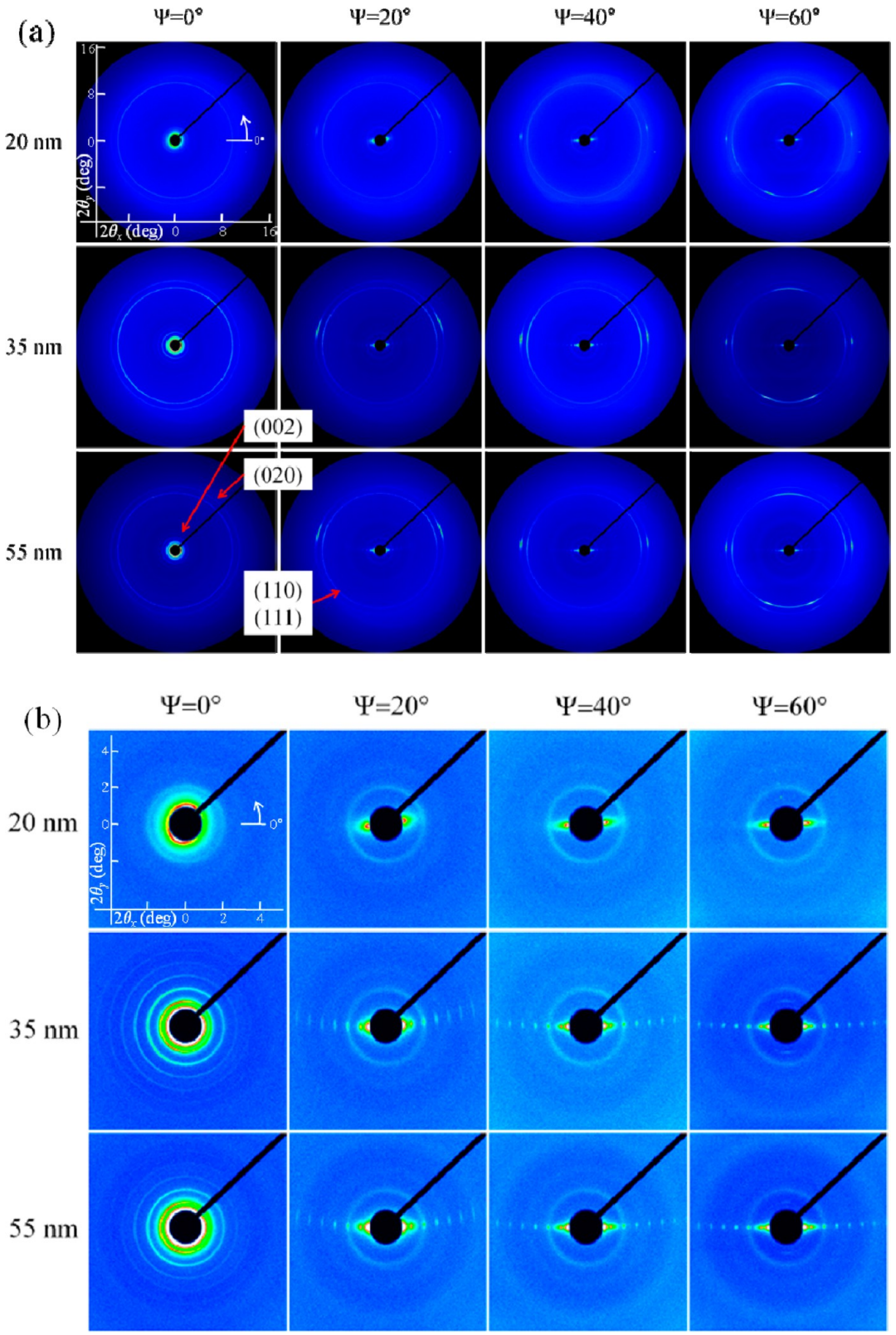


**Figure 4.** X-ray diffraction patterns of C41 crystallized in the surface-modified AAOs with different nanopore diameters; (a) full scale and (b) zoom of (a) to show low $2\theta$ region.

axes of the cylindrical nanopores parallel with respect to the incident X-ray beam. The XRD patterns at $\psi = 0°$ exhibit the typical ones for randomly oriented C41 crystals. As marked in the Figure 3, the diffraction rings from the center of the patterns are from (002), (110)/(111), and (020) planes for orthorhombic C41 crystal. With increasing the rotation angle of $\psi$, the asymmetric patterns that are originated from the curvature of the Ewald sphere were observed against the horizontal line through the beam center. As shown in Scheme 3, the Ewald sphere has curved surface, while diffraction


dx.doi.org/10.1021/jp308678b | J. Phys. Chem. B XXXX, XXX, XXX−XXX

**Scheme 3. Schematic Illustration of Intersection between the Ewald Sphere and Diffraction Rings (a) at $\psi = 0°$ and (b) with Increase of $\psi$[a]**

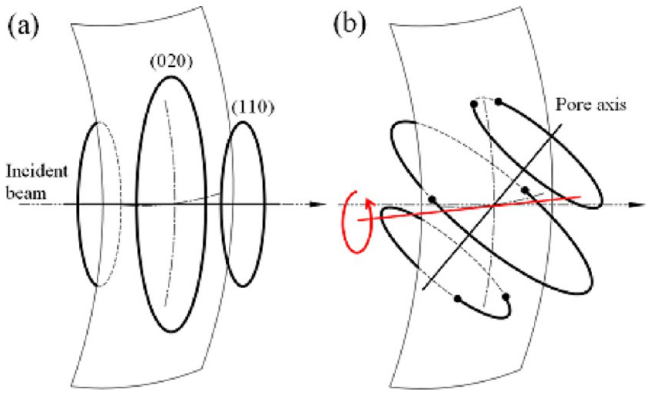


[a]The vertical and the horizontal alternated long and short dash line on the Ewald sphere is the meridian and the equator, respectively.

patterns lay in the flat plane. Therefore, at $\psi = 0°$ the diffraction rings from oriented crystals do not intersect with the Ewald sphere without artifacts, as shown in Scheme 3a. If the samples are rotated with respect to the horizontal rotating axis, the position of the patterns becomes asymmetric against the horizontal line from the intersection between the flat plane and the curved surface as shown in Scheme 3b. The (002) diffraction peaks approached to the equator, as $\psi \sim 60°$. The (020) reflections were also located near the equator when $\psi = 60°$. However, with the increase of $\psi$, (110)/(111) reflections touched four horizontally asymmetric positions on the detector. These $\psi$-dependent XRD patterns suggest that the *b*- and *c*-axes of orthorhombic C41 crystals are preferentially aligned perpendicular to the pore axis, while the *a*-axis lies parallel to the pore axis. In addition, the azimuthal broadening of the diffraction peaks was found with the increase of pore diameter, resulting from less severe confinement imposed upon the C41 crystals in larger nanopores.

Figure 4 displays the XRD patterns of C41 crystallized in the surface-modified alumina nanopores. The orthorhombic (002) reflection in the XRD patterns at $\psi = 0°$ for C41 in the surface-modified AAOs was also observed, as in the one of C41 in the pristine AAOs. The patterns of (002) reflection approached to the equator with the increase of $\psi$ from 0 to 60°. But the patterns of (110)/(111) and (020) reflections of C41 in the surface-modified AAOs were different from those for C41 in the pristine AAOs. The (110)/(111) reflections were located asymmetrically near the equator with weak intensity. The (020) diffraction also approached the equator with increasing $\psi$. However, weak (020) reflections of the XRD patterns of C41 in the surface-modified AAOs appeared additionally on the four

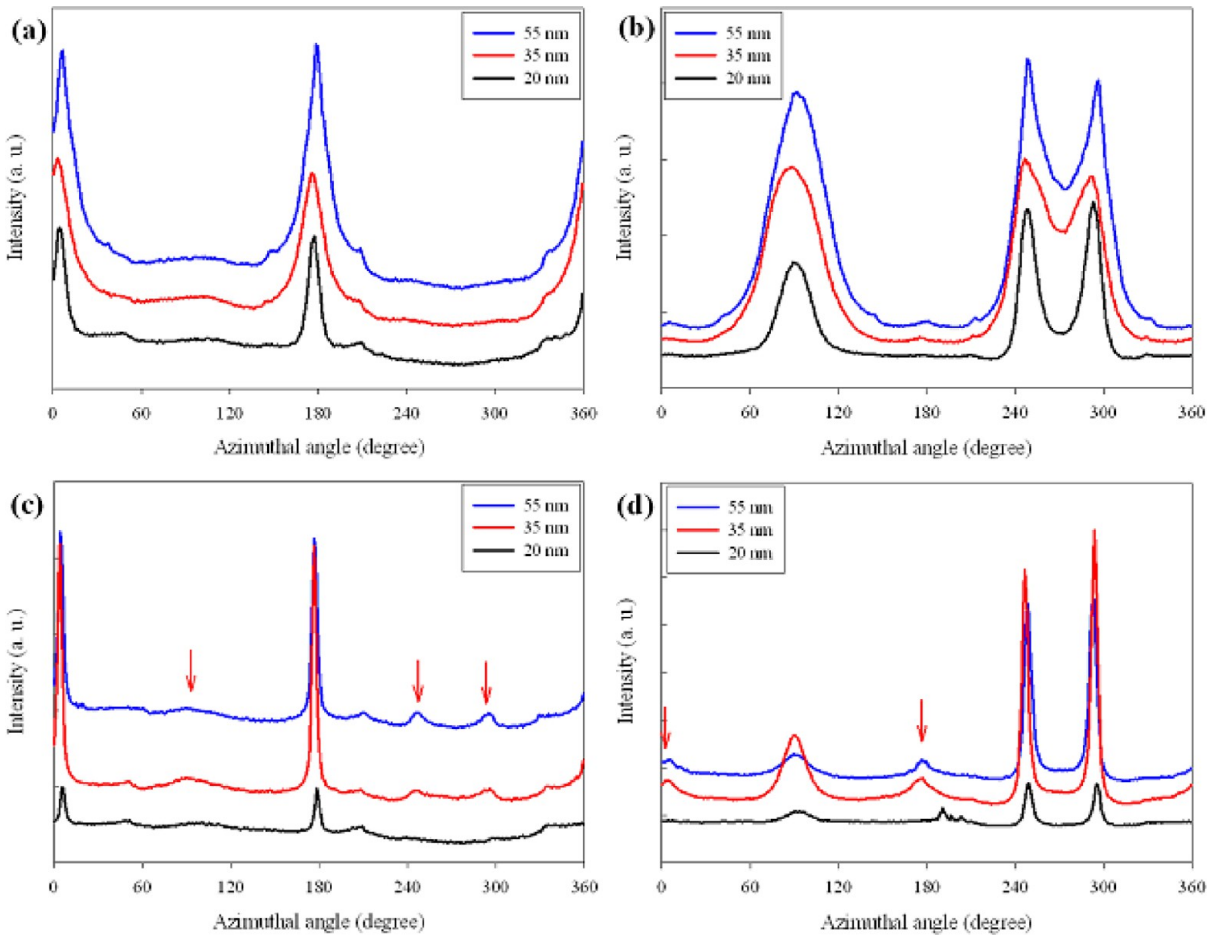


**Figure 5.** Azimuthally scanned 1D plots of (a) (020) reflection of C41 in the pristine AAOs, (b) (110)/(111) reflection of C41 in the pristine AAOs, (c) (020) reflection of C41 in the surface-modified AAOs, and (d) (110)/(111) reflection of C41 in the surface-modified AAOs at $\psi = 60°$, which are obtained using 2D X-ray diffraction patterns of Figures 3 and 4.


dx.doi.org/10.1021/jp308678b | J. Phys. Chem. B XXXX, XXX, XXX–XXX

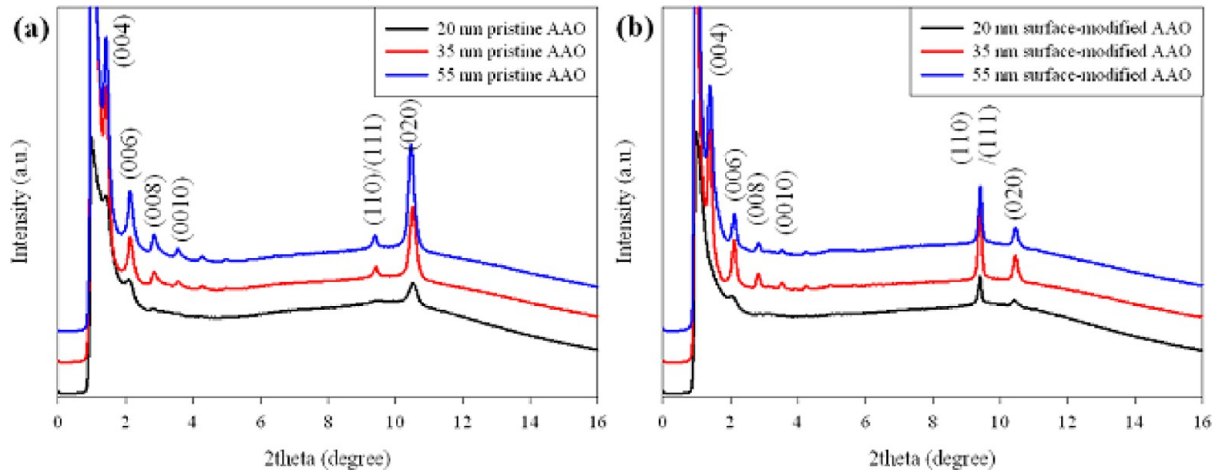


**Figure 6.** Circular average 1D plots of X-ray diffraction patterns of C41 at $\psi = 0°$; (a) in Figure 3 and (b) in Figure 4.

horizontally asymmetric positions. It can be clearly seen in the azimuthally scanned 1D plots of (110)/(111) and (020) reflection from C41 in the pristine and surface-modified AAOs, as shown in Figure 5. From the $\psi$-dependent XRD patterns for C41 in the surface-modified AAOs, it is suggested that there exist two different orientations for C41 crystals developed in the surface-modified AAOs. One orientation is identical to the C41 in the pristine AAOs, as the *b*- and *c*-axes of orthorhombic C41 crystals are aligned perpendicular to the pore axis and the *a*-axis lies parallel to the pore axis. Another orientation is the (110) plane of C41 crystals that is aligned parallel to the nanopore axis, while the *c*-axis lies perpendicular to the pore axis.

The preferred orientation of C41 crystals in nanopores is directed in the presence of cylindrical nanoscopic confinement. Nucleation of crystal, the dominant crystallization mechanism, is believed to influence the crystal orientation by the confinement. It is conjectured that confinements affect the initial formation of crystal and preferential orientations of crystals are obtained. Crystal growth is also thought to be influenced by the presence of nanoscopic cylindrical confinement, although it is not a dominant crystallization mechanism. For the crystallization of polyethylene in bulk, which is a long-chain polymer but has the same backbone as in C41, the crystals grow along both ⟨110⟩ and ⟨100⟩ directions.[44,45] The crystal growth rate of ⟨110⟩ direction is faster than that of ⟨100⟩ direction above 80 °C. It can be explained that the crystallites of polyethylene confined in nanoporous AAOs were developed preferentially along the ⟨110⟩ direction and the *b*-axis of crystals was parallel to the pore axis.[19] Taking into account the fact that the *a*- and *b*-axes of C41 are equivalent to the *b*- and *a*-axes of polyethylene, respectively, it is thought that the C41 crystals in the pristine AAOs are developed preferentially along the ⟨110⟩ direction and lay elongated along the *a*-axis. It was reported by researchers that the fastest-growth direction of low molecular weight materials[46,47] or polymers[48,49] confined in the nanoscopic space aligned parallel with the pore axis. When inhibition by a foreign material[47] or surface energy[9] occurs, the new fastest-growth direction determines preferential orientation and aligns parallel to the pore axis. It is expected that in the surface-modified AAOs the growth of C41 crystals are suppressed along the ⟨110⟩ direction owing to the low surface energy. But they are developed preferentially along the ⟨010⟩ direction at relatively low temperature. The growth along the ⟨010⟩ direction is thought to cause the tilting of *a*- and *b*-axes as well as to align the (110)/(111) plane parallel to the nanopore axis. Circularly averaged 1D plots at $\psi = 0°$ of Figures 3 and 4 are presented in Figure 6. The difference of intensity ratio between reflections of (110)/(111) and (020) is caused by the perturbed orientations as discussed above. Scheme 4 shows the illustration of C41 crystals developed in the nanopores of the pristine and the surface-modified AAOs.

**Scheme 4. Illustration of C41 Crystals Developed in the Pristine AAO (A) and Surface-Modified AAO (b)**

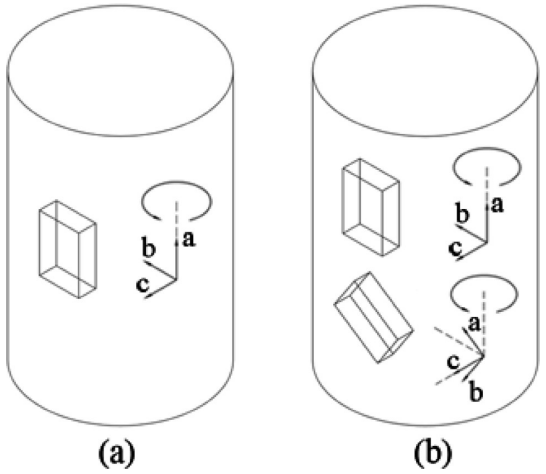


Two important findings from XRD experiments are (1) formation of fully extended crystallites of C41 in nanopores and (2) surface property-dependent crystal orientation. The *d*-spacings calculated from diffraction peaks such as (004), (006), (008), and (0010) at low $2\theta$ region were 27.2, 18.0, 13.6, and 10.9 Å, respectively. The appearance of those higher order peaks, especially like (0010) and (008), reveals that C41 crystallized with fully extended crystallites.[25,29,50] Associated with the surface property-dependent crystallization behaviors shown in DSC cooling curves, there seems to be preferred orientation of C41 crystals that formed at each of the temperature ranges. Considering the XRD intensity and crystallization DSC curves, crystal orientation in which the *a*-axis is parallel with the pore axes is preferred for C41 crystals


dx.doi.org/10.1021/jp308678b | J. Phys. Chem. B XXXX, XXX, XXX−XXX

formed in the pristine AAOs, while another orientation in which (110) is parallel with the pore axis becomes dominant for C41 crystals developed in the surface-modified AAOs at the higher crystallization temperature range. Especially in the surface-modified AAO with the diameter of 20 nm, disappearance of crystallization of the higher-temperature ranges corresponds to the existence of one preferred orientation found in the XRD pattern that shows the *a*-axis parallel with the pore axis. Such preferred orientation is thought to result from a different crystallization mechanism owing to the difference in surface energies between the pristine and surface-modified AAOs.

## CONCLUSIONS

We investigated the effects of the confinement and the surface property on the crystallization behavior and the crystal orientation of C41 confined in the nanoscopic cylindrical geometry. From the nonisothermal crystallization experiments, C41 in the pristine AAOs crystallized at lower-temperature ranges in comparison with bulk crystallization and exhibited the decreased Avrami exponents. These result from the dominant nucleation and the dimensional restriction of crystal growth due to the AAOs. For the crystallization of C41 in the surface-modified AAOs, the crystallization at the higher temperature zone was restricted, but at the lower temperature zone it was enhanced. It is quite obvious that the crystallization is strongly influenced by the degree of confinement and the nature of the template surface. The crystal orientation was also affected by both the nanoscopic confinement and the surface modification. In the nanopores of the pristine AAOs, the *a*-axis of the orthorhombic C41 crystals was parallel to the pore axis and the *b*- and *c*-axes were perpendicular to the pore axis. The C41 crystals confined in the nanopores of the surface-modified AAOs exhibited two kinds of orientations. One is identical to those in the pristine AAOs and the other orientation was that the (110) plane of orthorhombic crystals was parallel to the pore axis while the *c*-axis was perpendicular to the pore axis. These preferential orientations of C41 crystals in the nanopores can be explained by the restriction of crystal growth by the geometrical confinement as well as the surface energy.

## ASSOCIATED CONTENT

### Supporting Information

Contact angle, SEM images of nanopores before and after surface modification, and SEM cross-sectional images of AAO after infiltration of C41. This material is available free of charge via the Internet at http://pubs.acs.org.

## AUTHOR INFORMATION

### Corresponding Author

*E-mail: shin@snu.ac.kr.

### Notes

The authors declare no competing financial interest.

## ACKNOWLEDGMENTS

This work was supported by Construction Technology Innovation Program funded by Korea Ministry of Land, Transportation, and Maritime Affairs (MLTM) (400-20110090). The authors appreciate the experimental support by the staffs at the 4C beamline of Pohang Light Source.

## REFERENCES

(1) Keddi, J. L.; Jones, R. A. L.; Cory, R. A. Size-Dependent Depression of the Glass Transition Temperature in Polymer Films. *Europhys. Lett.* **1994**, *27*, 59−64.
(2) Wallace, W. E.; Van Zanten, J. H.; Wu, W. L. Influence of an Impenetrable Interface on a Polymer Glass-Transition Temperature. *Phys. Rev. E* **1995**, *52*, R3329−R3332.
(3) Fakhraai, Z.; Forrest, J. A. Measuring the Surface Dynamics of Glassy Polymers. *Science* **2008**, *319*, 600−604.
(4) Woo, E.; Huh, J.; Jeong, Y. G.; Shin, K. From Homogeneous to Heterogeneous Nucleation of Chain Molecules under Nanoscopic Cylindrical Confinement. *Phys. Rev. Lett.* **2007**, *98*, 136103.
(5) Duran, H.; Steinhart, M.; Butt, H.; Floudas, G. From Heterogeneous to Homogeneous Nucleation of Iisotactic Poly(propylene) Confined to Nanoporous Alumina. *Nano Lett.* **2011**, *11*, 1671−1675.
(6) Li, M.; Wu, H.; Huang, Y.; Su, Z. Effects of Temperature and Template Surface on Crystallization of Syndiotactic Polystyrene in Cylindrical Nanopores. *Macromolecules* **2012**, *45*, 5196−5200.
(7) Shin, K.; Xiang, H. Q.; Moon, S. I.; Kim, T.; McCarthy, T. J.; Russell, T. P. Forcing a Polymer with Two Immiscible Parts into Cylindrical Pores Produced an Unusual Textured Surface that Provides New Templates for Material Fabrication. *Science* **2004**, *306*, 76.
(8) Diao, Y.; Harada, T.; Myerson, A. S.; Hatton, T. A.; Trout, B. L. The Role of Nanopore Shape in Surface-Induced Crystallization. *Nat. Mater.* **2011**, *10*, 867−871.
(9) Ha, J.-M.; Hamilton, B. D.; Hillmyer, M. A.; Ward, M. D. Alignment of Organic Crystals under Nanoscale Confinement. *Cryst. Growth Des.* **2012**, *12*, 4494−4504.
(10) Shin, K.; Obukhov, S.; Chen, J.-T.; Huh, J.; Hwang, Y.; Mok, S.; Dobriyal, P.; Thiyagarajan, P.; Russell, T. P. Enhanced Mobility of Confined Polymers. *Nat. Mater.* **2007**, *6*, 961−965.
(11) Despotopoulou, M. M.; Miller, R. D.; Rabolt, J. F.; Frank, C. W. Polymer Chain Organization and Orientation in Ultrathin Films: A Spectroscopic Investigation. *J. Polym. Sci., Part B: Polym. Phys.* **1996**, *34*, 2335−2349.
(12) Despotopoulou, M. M.; Frank, C. W.; Miller, R. D.; Rabolt, J. F. Kinetics of Chain Organization in Ultrathin Poly(di-n-hexylsilane) Films. *Macromolecules* **1996**, *29*, 5797−5804.
(13) Hong, S.; Macknight, W. J.; Russell, T. P.; Gido, S. P. Structural Evolution of Multilayered, Crystalline-Amorphous Diblock Copolymer Thin Films. *Macromolecules* **2001**, *34*, 2876−2883.
(14) Loo, Y. L.; Register, R. A.; Ryan, A. J. Polymer Crystallization in 25-nm Spheres. *Phys. Rev. Lett.* **2000**, *84*, 4120−4123.
(15) Zhu, L.; Cheng, S. Z. D.; Calhoun, B. H.; Ge, Q.; Quirk, R. P.; Thomas, E. L.; Hsiao, B. S.; Yeh, F. J.; Lotz, B. Crystallization Temperature-Dependent Crystal Orientations within Nanoscale Confined Lamellae of a Self-Assembled Crystalline-Amorphous Diblock Copolymer. *J. Am. Chem. Soc.* **2000**, *122*, 5957−5967.
(16) Huang, P.; Zhu, L.; Guo, Y.; Ge, Q.; Jing, A. J.; Chen, W. Y.; Quirk, R. P.; Cheng, S. Z. D.; Thomas, E. L.; Lotz, B.; Hsiao, B. S.; Avila-Orta, C. A.; Sics, I. Confinement Size Effect on Crystal Orientation Changes of Poly(ethylene oxide) Blocks in Poly(ethylene oxide)-b-polystyrene Diblock Copolymers. *Macromolecules* **2004**, *37*, 3689−3698.
(17) Hamilton, B. D.; Hillmyer, M. A.; Ward, M. D. Glycine Polymorphism in Nanoscale Crystallization Chambers. *Cryst. Growth Des.* **2008**, *8*, 3368−3375.
(18) Ha, J.-M.; Hillmyer, M. A.; Ward, M. D. Thermotropic Properties of Organic Nanocrystals Embedded in Ultrasmall Crystallization Chambers. *J. Phys. Chem. B* **2005**, *109*, 1392−1399.
(19) Shin, K.; Woo, E.; Jeong, Y. G.; Kim, C.; Huh, J.; Kim, K.-W. Crystalline Structures, Melting, and Crystallization ofLlinear Polyethylene in Cylindrical Nanopores. *Macromolecules* **2007**, *40*, 6617−6623.
(20) Massa, M. V.; Dalnoki-Veress, K. Homogeneous Crystallization of Poly(ethylene oxide) Confined to Droplets: The Dependence of the Crystal Nucleation Rate on Length Scale and Temperature. *Phys. Rev. Lett.* **2004**, *92*, 255509.

(21) Massa, M. V.; Carvalho, J. L.; Dalnoki-Veress, K. Direct Visualisation of Homogeneous and Heterogeneous Crystallisation in an Ensemble of Confined Domains of Poly(ethylene oxide). *Eur. Phys. J. E* **2003**, *12*, 111−117.
(22) Hammami, A.; Mehrotra, A. K. Non-Isothermal Crystallization Kinetics of *n*-Paraffins: Comparison of even-Numbered and odd-Numbered Normal Alkanes. *Thermochim. Acta* **1993**, *215*, 197−209.
(23) Hoffman, J. D. Growth Rate of Extended-Chain Crystals: Tthe Lateral Surface Free Energy of Pure *n*-$C_{94}H_{190}$ and a Fraction ~$C_{207}H_{416}$. *Macromolecules* **1985**, *18*, 772−786.
(24) Kraack, H.; Sirota, E. B.; Deutsch, M. Measurements of Homogeneous Nucleation in normal-Alkanes. *J. Chem. Phys.* **2000**, *112*, 6873−6884.
(25) Craig, S. R.; Hastie, G. P.; Roberts, K. J.; Sherwood, J. N. Investigation into the Structures of Some Normal Alkanes within the Homologous Series $C_{13}H_{28}$ to $C_{60}H_{122}$ using High-Resolution Synchrotron X-ray Powder Diffraction. *J. Mater. Chem.* **1994**, *4*, 977−981.
(26) Teckoe, J.; Bassett, D. C. The Crystallization Kinetics of Monodisperse $C_{98}H_{198}$ from the Melt. *Polymer* **2000**, *41*, 1953−1957.
(27) Oliver, M. J.; Calvert, P. D. Homogeneous Nucleation of *n*-Alkanes Measured by Differential Scanning Calorimetry. *J. Cryst. Growth* **1975**, *30*, 343−351.
(28) Turnbull, D.; Spaepen, F. Crystal Nucleation and the Crystal Melt Interfacial Tension in Linear Hydrocarbons. *J. Polym. Sci., Polym. Symp.* **1978**, *63*, 237−243.
(29) Ranby, B. G.; Morehead, F. F.; Walter, N. M. Morphology of *n*-Alkanes, Linear Polyethylene, and Isotactic Polypropylene Crystallized from Solution. *J. Polym. Sci.* **1960**, *44*, 349−367.
(30) Zhang, L.; Cho, H. S.; Li, F.; Metzger, R. M.; Doyle, W. D. Cellular Growth of Highly Ordered Porous Anodic Films on Aluminium. *J. Mater. Sci. Lett.* **1998**, *17*, 291−294.
(31) Masuda, H.; Yada, K.; Osaka, A. Self-Ordering of Cell Configuration of Anodic Porous Alumina with Large-Size Pores in Phosphoric Acid Solution. *Jpn. J. Appl. Phys* **1998**, *37*, L1340−L1342.
(32) Masuda, H.; Fukuda, K. Ordered Metal Nanohole Arrays Made by a Two-Step Replication of Honeycomb Structures of Anodic Alumina. *Science* **1995**, *268*, 1466−1468.
(33) Jessensky, O.; Muller, F.; Gosele, U. Self-Organized Formation of Hexagonal Pore Arrays in Anodic Alumina. *Appl. Phys. Lett.* **1998**, *72*, 1173−1175.
(34) Sun, Y. M.; Steinhart, M.; Zschech, D.; Adhikari, R.; Michler, G. H.; Gosele, U. Diameter-Dependence of the Morphology of PS-b-PMMA Nanorods Confined Within Ordered Porous Alumina Templates. *Macromol. Rapid Commun.* **2005**, *26*, 369−375.
(35) Lee, M. J.; Lee, N. Y.; Lim, J. R.; Kim, J. B.; Kim, M.; Baik, H. K.; Kim, Y. S. Antiadhesion Surface Treatments of Molds for High-Resolution Unconventional Lithography. *Adv. Mater.* **2006**, *18*, 3115−3119.
(36) Choi, M. K.; Yoon, H.; Lee, K.; Shin, K. Simple Fabrication of Asymmetric High-Aspect-Ratio Polymer Nanopillars by Reusable AAO Templates. *Langmuir* **2011**, *27*, 2132−2137.
(37) Ozawa, T. Kinetics of Non-Isothermal Crystallization. *Polymer* **1971**, *12*, 150−158.
(38) Hammami, A.; Mehrotra, A. K. Non-Isothermal Crystallization Kinetics of *n*-Paraffins with Chain Lengths between Thirty and Fifty. *Thermochim. Acta* **1992**, *211*, 137−153.
(39) Nakamura, K.; Watanabe, T.; Katayama, K.; Amano, T. Some Aspects of Nonisothermal Crystallization of Polymers. I. Relationship between Crystallization Temperature, Crystallinity, and Cooling Conditions. *J. Appl. Polym. Sci.* **1972**, *16*, 1077−1091.
(40) Nakamura, K.; Watanabe, T.; Katayama, K.; Amano, T. Some Aspects of Nonisothermal Crystallization of Polymers. II. Consideration of the Isokinetic Condition. *J. Appl. Polym. Sci.* **1973**, *17*, 1031−1041.
(41) Avrami, M. Kinetics of Phase Change. I General Theory. *J. Chem. Phys.* **1939**, *7*, 1103−1112.
(42) Wasiak, A. Kinetics of Polymer Crystallization in Non-Isothermal Conditions. *Chemtracts: Macromol. Chem.* **1991**, *2*, 211−245.
(43) Chatterjee, A. M.; Price, F. P.; Newman, S. Heterogeneous Nucleation of Crystallization of High Polymers from the Melt. III. Nucleation Kinetics and Interfacial Energies. *J. Polym. Sci., Part B: Polym. Phys.* **1975**, *13*, 2391−2400.
(44) Organ, S. J.; Keller, A. Fast Growth Rates of Polyethylene Single Crystals Grown at High Temperatures and Their Relevance to Crystallization Theories. *J. Polym. Sci., Part B: Polym. Phys.* **1986**, *24*, 2319−2335.
(45) Gedde, U. W. *Polymer Physics*; Chapman & Hall: London, 1995; p 138.
(46) Henschel, A.; Kumar, P.; Hofmann, T.; Knorr, K.; Huber, P. Preferred Orientation of *n*-Hexane Crystallized in Silicon Nanochannels: A Combined X-Ray Diffraction and Sorption Isotherm Study. *Phys. Rev. E* **2009**, *79*, 032601.
(47) Hamilton, B. D.; Weissbuch, I.; Lahav, M.; Hillmyer, M. A.; Ward, M. D. Manipulating Crystal Orientation in Nanoscale Cylindrical Pores by Stereochemical Inhibition. *J. Am. Chem. Soc.* **2009**, *131*, 2588−2596.
(48) Steinhart, M.; Goring, P.; Dernaika, H.; Prabhukaran, M.; Gosele, U.; Hempel, E.; Thurn-Albrecht, T. Coherent Kinetic Control over Crystal Orientation in Macroscopic Ensembles of Polymer Nanorods and Nanotubes. *Phys. Rev. Lett.* **2006**, *97*, 027801.
(49) Steinhart, M.; Stephan, S.; Wehrspohn, R. B.; Gosele, U.; Wendorff, J. H. Curvature-Directed Crystallization of Poly(vinylidene difluoride) in Nanotube Walls. *Macromolecules* **2003**, *36*, 3646−3651.
(50) Nene, S.; Karhu, E.; Flemming, R. L.; Hutter, J. L. A Diffusionless Transition in a Normal Alkane. *J. Cryst. Growth* **2009**, *311*, 4770−4777.